Position-Based Kinematics for 7-DoF Serial Manipulators with Global Configuration Control, Joint Limit and Singularity Avoidance

Carlos Faria[a,*], Flora Ferreira[b], Wolfram Erlhagen[c], Sérgio Monteiro[a], Estela Bicho[a,*]

[a] *Department of Industrial Electronics and Centre Algorithm, University of Minho, Guimarães 4800-058, Portugal*
[b] *Centre Algorithm, University of Minho, Guimarães 4800-058, and CIICESI, Polytechnic Institute of Porto, Felgueiras 4610-156, Portugal*
[c] *Department of Mathematics, University of Minho, Guimarães, 4800-058, Portugal*

Abstract

This paper presents a novel analytic method to uniquely solve inverse kinematics of 7 degrees-of-freedom manipulators while avoiding joint limits and singularities. Two auxiliary parameters are introduced to deal with the self-motion manifolds: the global configuration (GC), which specifies the branch of inverse kinematics solutions; and the arm angle (ψ) that parametrizes the elbow redundancy within the specified branch. The relations between the joint angles and the arm angle are derived, in order to map the joint limits and singularities to arm angle values. Then, intervals of feasible arm angles for the specified target pose and global configuration are determined, taking joint limits and singularities into account. A simple metric is proposed to compute the elbow position according to the feasible intervals. When the arm angle is determined, the joint angles can be uniquely calculated from the position-based inverse kinematics algorithm. The presented method does not exhibit the disadvantages inherent to the use of the Jacobian matrix and can be implemented in real-time control systems. This novel algorithm is the first position-based inverse kinematics algorithm to solve both global and local manifolds, using a redundancy resolution strategy to avoid singularities and joint limits.

Keywords: Analytic Inverse Kinematics, Configuration Control, Joint Limit Avoidance, Singularity Avoidance

1. Introduction

The optimum kinematic design for a 7 degrees-of-freedom (DoF) serial manipulator was proposed by Hollerbach in [1] as an alternative to 6 or less DoF manipulators, which have known difficulties overcoming obstructed workspaces and singularities. Due to their structural advantages in task performance, or to their human-likeness, 7-DoF serial manipulators are a trending subject with application over a wide range of research fields. Seven DoF manipulators are often referred to as redundant because the target pose is usually specified in task-space in three position and three orientation variables, which renders the inverse kinematics problem under-constrained.

The inverse kinematics for a redundant manipulator is an ill-posed and nonlinear problem. DeMers and Kreutz-Delgado [2, 3] subdivide this problem into local and global ill-posedness, related to the extra-degree of freedom and the multiple solution branches (affects redundant and non-redundant manipulators alike), respectively. The self-motion problem was previously examined through a topological perspective [4, 5]. It has been consensual among authors to split the problem into a finite set of manifolds in the configuration space (*c-bundles*), with the property that only one solution branch to the inverse kinematics problem may exist in each set. A *c-bundle* is homotopic and forward maps to the task space as a *w-sheet*. However, the pre-image of a *w-sheet* is a collection of *c-bundles* – as aforementioned – which are usually heterotopic with at least one co-regular surface delimiting its borders. Crossing a co-regular surface, to go from one *c-bundle* to the next invariably yields passing through a singular configuration. Avoiding singular configurations is often a requirement in task-space motion planning, a condition that motivates the algorithm proposed in this paper.

Within a *c-bundle* we find the self-motion manifold that derives from the extra DoF. Hollerbach [1] was the first to propose a description to the manifold as the angle between a reference plane and the plane formed by the shoulder, elbow and wrist – later called "arm angle" [6]. Other methods to describe the self-motion were later introduced [7, 8]. The redundant degree of freedom enables the manipulator to perform secondary tasks aside from reaching a

*Corresponding authors
Email addresses: cfaria@dei.uminho.pt (Carlos Faria), estela.bicho@dei.uminho.pt (Estela Bicho)

specific position and orientation [9], such as: singularities [10, 11, 12] and joint limits avoidance [13, 14, 15], obstacle avoidance [16, 17], minimise energy dissipation [18], enhance manipulability [19] and human-like motions [7, 20, 21].

The kinematic control of a redundant manipulator can be achieved by position- or velocity-based inverse methods, the latter being considered the standard approach to derive the inverse kinematic expressions of redundant manipulators [22, 23]. However, velocity-based control exhibits several disadvantages when compared to position-based control: i) computationally more expensive, returning only one solution [8, 24]; ii) difficult to map joint limits or configurations in the velocity domain [25]; iii) subject to error instability due to cumulative errors; iv) requires the pre-assignment of the Cartesian trajectory to follow [26]; v) Jacobian inversion consequent singularities [27]. Position-based closed-form solutions were deemed too difficult or impossible to derive due to the infinite number of joint configurations as a solution to the joint space manifold [26]. The introduction of auxiliary parameters to derive inverse kinematics expressions of redundant manipulators is a simple solution that greatly simplifies position-based methods [6, 28].

This paper proposes a novel analytic inverse kinematic method for non-offset 7 DoF anthropomorphic manipulators with global configuration control, and a redundancy resolution scheme to avoid singularity and joint limits. To address the local and global ill-posedness associated with the elbow's and configuration self-motion manifolds, two additional variables are introduced in the calculation of the kinematic expressions. The relationship between the joint angles and arm angles is studied to find singularities and to compute the values of the arm angle associated with joint limits. This analysis takes into account the specified joint configurations.

2. Related Work

Lee and Bejczy [26] presented, in 1991, the first approach towards closed-form inverse kinematics to achieve position-based control. They introduced an algorithm to parametrize redundant joints, transforming the redundant manipulator into a non-redundant image of itself. Their case studies support the premise of position-control advantages over Jacobian-based methods. The proposed algorithm can be theoretically applied to any kinematic structure. Nevertheless, the quality of the solution heavily depends on a proper selection of the redundant joints and on the geometric and algebraic analysis of the non-redundant manipulator image.

The technical report by Dahm and Joublin [27], in 1997, describes an analytic solution for the inverse kinematics problem of a 7-DoF serial manipulator with no offsets. The authors introduced the use of the arm angle in the computation of position-based inverse kinematics according to its geometric representation. The authors make an initial approach to map joint limits into the arm angle, as a strategy for joint limit avoidance. However, only the process of computing the arm angles relative to the wrist joint limit is described.

Tolani et al. [24] published in 2000 a set of inverse kinematic real-time algorithms for anthropomorphic limbs (7-DoF non-offset serial arm or leg). The authors present an interesting work using joint limit avoidance as a primary strategy for redundancy resolution. Two algorithms are introduced to address the inverse kinematics problem of under-constrained orientation and aiming, based on numerical approaches. However, the algorithms are not extended to a robotic structure nor the analytic expressions are derived.

The works of Tondu [7], Asfour and Dillmann [20], Kim and Rosen [21] all report analytic inverse kinematic solutions, based on position-control. With small differences when estimating the arm angle, these works take advantage of the manipulator's redundancy to enhance the human-likeness of the movement. Virtual joint limits are imposed to better imitate the human arm. These limitations, however, also simplify the inverse kinematics solution since they condition the possible configurations. Ultimately, solutions developed for applications under these constraints cannot be directly extended to manipulators with wider working ranges. Also, only Kim and Rosen [21] addressed the joint limits avoidance problem, by using an optimization routine that relies on estimated weight coefficients to distance from joint limits.

The works of Moradi and Lee [29] and Shimizu et al. [25] both describe a closed-form solution to inverse kinematics, and introduce a geometric and an analytic method to map the joint limits in the elbow self-motion manifold. Shimizu et al. developed a new concept to define the reference plane of the arm angle to avoid the algorithmic singularity, common to the technique of determining the reference plane from an arbitrary vector. Shimizu et al. derived the relation between the arm angle and each joint angle to map joint limits and singularities in the elbow-redundancy circle. The authors also describe an optimization method for joint limit avoidance. Nonetheless, the functions relating the joint and arm angles are not explored in their full domain since the joint limits imposed mimic the human-arm. Also, neither Shimizu's nor Moradi's work propose a method to deal with the global configuration manifold.

Singh and Claassens [30] and An et al. [8] describe analytic inverse kinematics solutions for 7-DoF redundant manipulators with non-zero joint offsets. These methods address the elbow's self-motion manifold, by means of

an additional parameter, either the arm angle or the theta-1 solution proposed in [7]. Only Singh and Claassens discuss the problem of avoiding joint limits and provide a method to calculate the arm angle intervals related to the limits of the joints 2, 4 and 6. However, as the authors explain, these constraints are a subset of the solution, since the remaining joint limits were not considered.

Yan et al. [11] present a closed-form inverse kinematics solution for redundant manipulators. They introduce a novel elbow-redundancy control approach based on dual-arm angle, to avoid situations where the reference plane degenerates to a line. No study was elaborated about the relation between arm angle and joint angles. On the other hand, the paper illustrates a novel approach towards the calculation of the reference plane, and how it affects the configuration control.

Kuhlemann et al. [28] have recently presented a robust inverse kinematics algorithm that controls the elbow-redundancy and the global configuration. The authors emphasize the importance of consistent joint configuration control to avoid jumping between configurations in a simple trajectory. Their work however, only addresses the inverse kinematic computation, making no allusion to joint limit or singularity avoidance methods.

In conclusion, and to the best of our knowledge, there is no work that combines the above-mentioned strategies. Hence, in this paper we present the first and single method capable of an unique position-based inverse kinematics solution, that includes a joint limit and singularity avoidance mechanism. The method can be applied to any 7-DoF non-offset anthropomorphic manipulator. It relies on a parametrization approach to solve the global configuration and local self-motion manifolds, and delivers a joint limit and singularity avoidance redundancy resolution based on the analysis of the relation between joints angles to the arm angle, mapped in the specified configuration space.

3. Analytic Kinematics

Seven-DoF non-offset anthropomorphic manipulators have a S-R-S (spherical-rotational-spherical) kinematic structure. One possible set of Denavit-Hartenberg (DH) parameters that describe the kinematic chain of a S-R-S serial manipulator are listed in Table 1.

Table 1: Classic Denavit-Hartenberg parameters of a 7-DoF anthropomorphic manipulator.

i	a_i	α_i	d_i	θ_i
1	0	$-\pi/2$	d_{bs}	θ_1
2	0	$\pi/2$	0	θ_2
3	0	$\pi/2$	d_{se}	θ_3
4	0	$-\pi/2$	0	θ_4
5	0	$-\pi/2$	d_{ew}	θ_5
6	0	$\pi/2$	0	θ_6
7	0	0	d_{wf}	θ_7

Each θ_i represents the i^{th} joint position variable, which is physically limited by the joint mechanical upper-limit θ_i^u and lower limit $\theta_i^l, i \in \{1, ..., 7\}$. The column d_i describes the kinematic link lengths between: (b)ase, (e)lbow, (w)rist and (f)lange (see Figure 1).

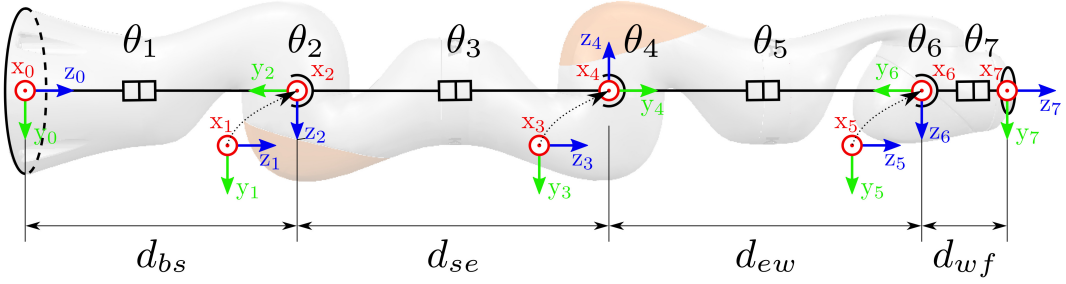

Figure 1: Manipulator generic structure, joint variables and DH frames assigned. The 7-DoF manipulator model of LBR iiwa 7 R800 from KUKA AG is used to depict the shape of an anthropomorphic arm without offsets.

The forward kinematics problem is easily solved once the DH parameters are determined. Four parameters are assigned to each joint, which convert to a transformation matrix that establishes the relation between one assigned

reference frame $(i-1)$ and the next (i),

$$ {}^{i-1}\mathbf{T}_i = \begin{bmatrix} \cos\theta_i & -\sin\theta_i\cos\alpha_i & \sin\theta_i\sin\alpha_i & a_i\cos\theta_i \\ \sin\theta_i & \cos\theta_i\cos\alpha_i & -\cos\theta_i\sin\alpha_i & a_i\sin\theta_i \\ 0 & \sin\alpha_i & \cos\alpha_i & d_i \\ 0 & 0 & 0 & 1 \end{bmatrix}. \tag{1} $$

The product of these matrices from the base to the flange, ${}^0\mathbf{T}_7 = {}^0\mathbf{T}_1\,{}^1\mathbf{T}_2\,{}^2\mathbf{T}_3\,{}^3\mathbf{T}_4\,{}^4\mathbf{T}_5\,{}^5\mathbf{T}_6\,{}^6\mathbf{T}_7$, returns the manipulator's pose in task space.

3.1. Self-Motion Parameters

To address the global and local self-motion manifolds, two additional parameters are introduced in the calculation of the inverse kinematics. The first parameter – Global Configuration (GC) – uniquely specifies the branch of the inverse kinematics solutions for the global configuration manifold. The second parameter – arm angle (ψ) – introduced by Hollerbach [1], indicates the elbow position in the redundancy circle. Both the GC and ψ variables are directly determined in the forward kinematics problem from the joint angles, and are passed as parameters to the proposed inverse kinematics algorithm.

The Global Configuration GC_k parameter is split into 3 variables that express the sign of the joint angle coordinates at the shoulder (GC_2), elbow (GC_4) and wrist (GC_6). These variables subsequently exert control over the manipulator's arrangement in space. The GC_k is given by,

$$ GC_k = \begin{cases} 1, & \text{if } \theta_k \geq 0 \\ -1, & \text{if } \theta_k < 0. \end{cases}, \forall k \in \{2,4,6\}. \tag{2} $$

The manipulator's arrangement in space is directly affected by the GC_k at the shoulder, elbow and wrist.

The arm angle, represents the angle formed by the shoulder-elbow-wrist plane (SEW) and the reference plane (SE^{v}W), as shown in Figure 2. The elbow redundancy depends solely on the structure of the manipulator and on the shoulder-wrist vector. The center of the ψ circle is located at half the distance along the straight line connecting the shoulder to the wrist, and its curve is inscribed in the plane defined by the shoulder-wrist vector.

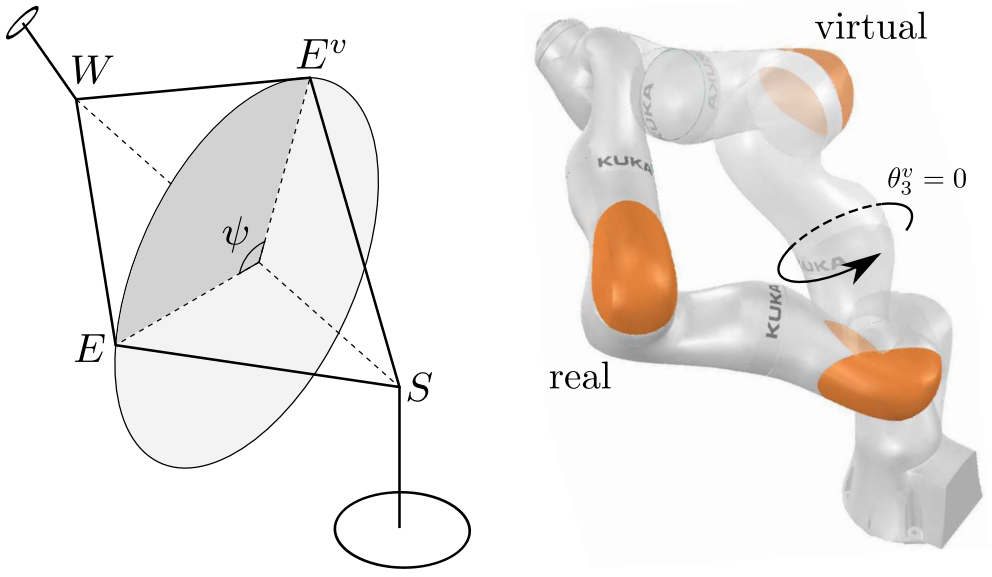

(a) Representation of the arm angle (ψ), as the angle between the real (E) and virtual elbow (E^v) in the redundancy circle.

(b) Configuration of the real and virtual manipulator at the same pose.

Figure 2: The "real manipulator" depicts a 7-DoF manipulator at an arbitrary pose. The "virtual manipulator" is the non-redundant (6-DoF) replica of the same manipulator reaching the same pose. The real manipulator is transformed into the virtual manipulator by blocking the 3^{th} joint at zero ($\theta_3 = 0$).

The selection of the reference plane is not straightforward and has been a topic of discussion in several works (see e.g. [25, 11]). The first approach [6, 27] was to define the reference plane based on the shoulder and wrist

positions, and an arbitrary vector. Whilst this method is the easiest to compute and establishes a clear relation between the arm angle and the task space, it also raises algorithmic singularities that derive from the possibility of the arbitrary vector being collinear with the shoulder-wrist vector. In this case, the reference plane can no longer be determined since the vectors that describe the plane are linearly dependent.

Shimizu et al. [25] introduced a workaround to the algorithmic singularity by defining the reference plan based on a virtual manipulator that is a non-redundant image of the original 7-DoF manipulator, with $\theta_3 = 0$. If no joint limits are imposed to the virtual manipulator, provided a target pose within its workspace, one can find a finite set of solutions for the inverse kinematics problem. These solutions, depend on the virtual manipulator configuration, which was not addressed in the referred paper.

Yan et al. [11] presented the "dual arm angle" algorithm, which uses two perpendicular arbitrary vectors to define the reference plane, following the same approach as Kreutz-Delgado et al. [6]. The algorithm follows the principle that the shoulder-wrist vector cannot be collinear with both arbitrary vectors at the same time, so when the singularity occurs for one of the arbitrary vectors, they switch to the other one to generate the reference plane.

To develop an algorithm that solves global configuration self-motion along with the elbow redundancy, it should guarantee that: 1) the definition of the reference plane needs to account for the joint configuration, the *GC* parameter; 2) the homotopic property within *c-bundles* should be extended to the nullspace definition – function of ψ. That is, any function in task-space should be continuously deformed into a function of the ψ parameter for a specific global configuration branch. The method from Yan et al. satisfies the first premise, but not the second. For this reason, we extended the method originally proposed by Shimizu et al. [25] to consider the robot joint configuration.

3.2. Elbow redundancy

The arm angle, ψ, is the angle between the vectors normal to the real manipulator SEW plane and the virtual (non-redundant) manipulator SE^{v}W plane (Figure 2). There is however a small caveat to the statement, since the same plane can be defined by both its vector and its negative vector. This indetermination is relevant to our problem because the definition of the reference SEW plane vector depends on the global configuration of the virtual manipulator, i.e. if the elbow is upwards or downwards. To uniquely determine a reference plane vector, we associate the robot configuration variable *GC* to the calculation of the reference plane.

It is easy to prove that the shoulder and wrist positions are common to the real and virtual robot for the same target pose (Figure 2). Therefore, we only need the elbow position of the virtual manipulator to find the reference plane and consequently calculate ψ. Inverse kinematic expressions for the 6-DoF virtual manipulator are applied to discover its elbow position. The joint positions of the virtual manipulator will be represented by a superindex θ_i^v.

Let the target pose be represented by a transformation matrix ${}^0\mathbf{T}_7$, that combines a position component ${}^0\mathbf{p}_7 \in \mathbb{R}^3$ and a rotation component ${}^0\mathbf{R}_7 \in SO(3)$. To simplify the notation of the following equations, we list the vectors from: base to shoulder (${}^0\mathbf{p}_2$), shoulder to elbow (${}^2\mathbf{p}_4$), elbow to wrist (${}^4\mathbf{p}_6$) and wrist to flange (${}^6\mathbf{p}_7$) according to the DH parameters:

$$
\begin{aligned}
{}^0\mathbf{p}_2 &= \begin{bmatrix} 0 & 0 & d_{bs} \end{bmatrix}^T \\
{}^2\mathbf{p}_4 &= \begin{bmatrix} 0 & d_{se} & 0 \end{bmatrix}^T \\
{}^4\mathbf{p}_6 &= \begin{bmatrix} 0 & 0 & d_{ew} \end{bmatrix}^T \\
{}^6\mathbf{p}_7 &= \begin{bmatrix} 0 & 0 & d_{wf} \end{bmatrix}^T .
\end{aligned}
$$

The virtual elbow joint (θ_4^v) is the first to be calculated, since it only depends on the manipulator's kinematic structure and on the shoulder-wrist vector. The shoulder-wrist vector is calculated from:

$$
{}^2\mathbf{p}_6 = {}^0\mathbf{p}_7 - {}^0\mathbf{p}_2 - \left({}^0\mathbf{R}_7 \, {}^6\mathbf{p}_7\right) \tag{3}
$$

and θ_4^v is computed using the law of cosines

$$
\theta_4^v = GC_4 \arccos\left(\frac{\left\| {}^2\mathbf{p}_6 \right\|^2 - (d_{se})^2 - (d_{ew})^2}{2 \; d_{se} \; d_{ew}} \right). \tag{4}
$$

The elbow configuration variable (GC_4) – the signal of the 4^{th} joint angle – is required to uniquely define the reference plane (4).

Since θ_3^v is 0, the shoulder-elbow vector (${}^2\mathbf{p}_4$), as well as the elbow-wrist vector (${}^4\mathbf{p}_6$) are aligned in the xy-plane. The joint θ_1^v is thus responsible for moving the virtual arm to the wrist x- and y- position coordinates.

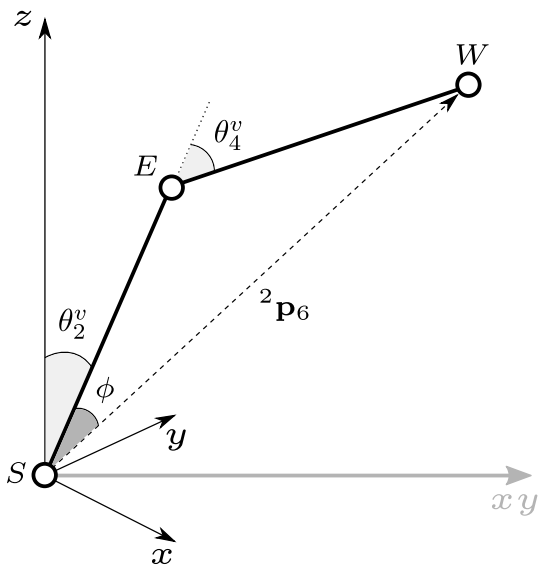

Figure 3: Representation of the virtual manipulator and variables required for the θ_2^v calculation.

However, if the shoulder-wrist vector (${}^2\mathbf{p}_6$) is aligned to the z-axis of joint 1 (${}^0\mathbf{R}_{1,z}$), then joint 1 is no longer defined and an algorithmic singularity occurs. Hence, the calculation of θ_1^v branches into,

$$\theta_1^v = \begin{cases} \text{atan2}\left({}^2\mathbf{p}_{6,y}, {}^2\mathbf{p}_{6,x}\right), & \text{if } \left\|{}^2\mathbf{p}_6 \times {}^0\mathbf{R}_{1,z}\right\| > 0 \\ 0, & \text{if } \left\|{}^2\mathbf{p}_6 \times {}^0\mathbf{R}_{1,z}\right\| = 0 \end{cases}. \tag{5}$$

The virtual shoulder joint θ_2^v is the last missing variable to find the virtual elbow position. As can be seen in Figure 3, ϕ can be calculated from the law of cosines:

$$\phi = \arccos\left(\frac{(d_{se})^2 + \left\|{}^2\mathbf{p}_6\right\|^2 - (d_{ew})^2}{2\ d_{se}\ \left\|{}^2\mathbf{p}_6\right\|}\right), \tag{6}$$

and the value of θ_2^v, which depends on the elbow configuration, is:

$$\theta_2^v = \text{atan2}\left(\sqrt{({}^2\mathbf{p}_{6,x})^2 + ({}^2\mathbf{p}_{6,y})^2},\ {}^2\mathbf{p}_{6,z}\right) + GC_4\ \phi. \tag{7}$$

With θ_1^v, θ_2^v, θ_3^v and θ_4^v we can calculate the pose of the virtual elbow from the base (${}^0\mathbf{T}_4^v$) using the forward kinematics (1). The normal vector to the plane ($\mathbf{v}_{sew}^v$) is now calculated as the cross product of the unit vectors that link shoulder-elbow and shoulder-wrist:

$$\mathbf{v}_{sew}^v = \left(\frac{{}^0\mathbf{p}_4^v\ -\ {}^0\mathbf{p}_2^v}{\left\|{}^0\mathbf{p}_4^v\ -\ {}^0\mathbf{p}_2^v\right\|}\right) \times \left(\frac{{}^0\mathbf{p}_6^v\ -\ {}^0\mathbf{p}_2^v}{\left\|{}^0\mathbf{p}_6^v\ -\ {}^0\mathbf{p}_2^v\right\|}\right). \tag{8}$$

The normal vector to the real arm SEW plane ($\mathbf{v}_{sew}$) is calculated using the same formula with the position of the real elbow instead,

$$\mathbf{v}_{sew} = \left(\frac{{}^0\mathbf{p}_4\ -\ {}^0\mathbf{p}_2}{\left\|{}^0\mathbf{p}_4\ -\ {}^0\mathbf{p}_2\right\|}\right) \times \left(\frac{{}^0\mathbf{p}_6\ -\ {}^0\mathbf{p}_2}{\left\|{}^0\mathbf{p}_6\ -\ {}^0\mathbf{p}_2\right\|}\right). \tag{9}$$

Let $\psi \in [-\pi, \pi]$ and in particular ψ be 0 at the reference plane. The sign of the arm angle parameter is determined as,

$$sg_\psi = \text{sgn}\left[\left(\widehat{\mathbf{v}_{sew}^v} \times \widehat{\mathbf{v}_{sew}}\right) \cdot {}^2\mathbf{p}_6\right] \tag{10}$$

and ψ as,

$$\psi = sg_\psi\ \arccos\left(\widehat{\mathbf{v}_{sew}^v} \cdot \widehat{\mathbf{v}_{sew}}\right). \tag{11}$$

Since the arm angle, ψ, is now determined, along with the joint configuration (GC) and the final robot pose (${}^0\mathbf{T}_7$), there exists a full description of the robot configuration in task space, which maps to an unique manipulator configuration in joint space.

4. Inverse Kinematics

The described inverse kinematics algorithm is based on the standard approach of dividing the manipulator into the upper and lower arm, responsible for positioning and orientation respectively. In the same way that forward kinematics computes the final pose (${}^0\mathbf{T}_7$) and self-motion parameters (ψ, GC) from the joint positions, reciprocally, the inverse kinematics requires these three variables to generate a set of joint positions.

The first step consists of determining the shoulder-wrist vector (${}^2\mathbf{p}_6$). The same equation used for the virtual manipulator (3) can be applied for the real robot, since the shoulder and wrist positions are coincident. Moreover, because the shoulder to wrist vector is the same, also the elbow joint (θ_4) can be calculated from (4).

The θ_4 is the only joint angle that does not depend on ψ. In order to determine the other joint angles, we need to find the position of the real manipulator elbow. To do so, first we calculate the virtual elbow pose at the reference plane (${}^0\mathbf{T}_4^v$), following the algorithm described in section 3.2. The real elbow pose is no more than the virtual elbow pose, rotated around the shoulder-wrist axis (${}^2\mathbf{p}_6$) of ψ,

$$ {}^0\mathbf{R}_4 = {}^0\mathbf{R}_\psi \; {}^0\mathbf{R}_4^v \tag{12} $$

which is equivalent to

$$ {}^0\mathbf{R}_3 = {}^0\mathbf{R}_\psi \; {}^0\mathbf{R}_3^v, \tag{13} $$

because θ_4 is the same in the virtual and the real manipulator, hence ${}^3\mathbf{R}_4^v = {}^3\mathbf{R}_4$.

The elbow redundancy rotation matrix (${}^0\mathbf{R}_\psi$) codes the rotation of the angle ψ around the shoulder-wrist vector (${}^2\mathbf{p}_6$), Figure2a. It is calculated using the *Rodrigues's rotation formula* in matrix notation,

$$ {}^0\mathbf{R}_\psi = \mathbf{I}_3 + \sin(\psi)\left[\widehat{{}^2\mathbf{p}_6}\times\right] + (1-\cos(\psi))\left[\widehat{{}^2\mathbf{p}_6}\times\right]^2 \tag{14} $$

where $\left[\widehat{{}^2\mathbf{p}_6}\times\right]$ is the cross-product matrix for the unit vector $\widehat{{}^2\mathbf{p}_6}$.

Substituting (14) into (13) and following the notation in Shimizu et al. [25], ${}^0\mathbf{R}_3$ can be obtained in terms of three auxiliary matrices $\mathbf{A}_s$, $\mathbf{B}_s$ and $\mathbf{C}_s$,

$$ {}^0\mathbf{R}_3 = \mathbf{A}_s \sin(\psi) + \mathbf{B}_s \cos(\psi) + \mathbf{C}_s \tag{15} $$

where,

$$ \mathbf{A}_s = \left[\widehat{{}^2\mathbf{p}_6}\times\right] \; {}^0\mathbf{R}_3^v $$

$$ \mathbf{B}_s = -\left[\widehat{{}^2\mathbf{p}_6}\times\right]^2 \; {}^0\mathbf{R}_3^v $$

$$ \mathbf{C}_s = \left[\widehat{{}^2\mathbf{p}_6} \; \widehat{{}^2\mathbf{p}_6}^T\right] \; {}^0\mathbf{R}_3^v. $$

The real values of θ_1, θ_2 and θ_3 are now determined analytically by combining the elements[1] of the ${}^0\mathbf{R}_3(\theta_{1,2,3})$ matrix – derived from DH parameters – in trigonometric operations,

$$ {}^0\mathbf{R}_3(\theta_{1,2,3}) = \begin{bmatrix} * & \cos\theta_1 \sin\theta_2 & * \\ * & \sin\theta_1 \sin\theta_2 & * \\ -\sin\theta_2\cos\theta_3 & \cos\theta_2 & -\sin\theta_2\sin\theta_3 \end{bmatrix}. \tag{16} $$

The $*$ symbol indicates omitted elements of the matrix, which are not required for joint position calculations.

It is important to note that these joint angles are subject to the global configuration parameter GC, thus:

$$ \begin{aligned} \theta_1 = \operatorname{atan2}\big(&GC_2[a_{s22}\sin\psi + b_{s22}\cos\psi + c_{s22}]\,, \\ &GC_2\,[a_{s12}\sin\psi + b_{s12}\cos\psi + c_{s12}]\big) \end{aligned} \tag{17} $$

[1] The notation m_{ij} is used to specify the element of the $\mathbf{M}$ matrix at the i^{th} line and j^{th} column

$$\theta_2 = GC_2 \arccos\left(a_{s32}\sin\psi + b_{s32}\cos\psi + c_{s32}\right) \tag{18}$$

$$\theta_3 = \operatorname{atan2}\left(GC_2[-a_{s33}\sin\psi - b_{s33}\cos\psi - c_{s33}],\; GC_2\left[-a_{s31}\sin\psi - b_{s31}\cos\psi - c_{s31}\right]\right). \tag{19}$$

Once we know the rotation matrix relative to the shoulder joints (${}^0\mathbf{R}_3$), it is straightforward to compute the rotation matrix of the wrist joints (${}^4\mathbf{R}_7$)

$${}^4\mathbf{R}_7 = \mathbf{A}_w\sin(\psi) + \mathbf{B}_w\cos(\psi) + \mathbf{C}_w \tag{20}$$

where,

$$\mathbf{A}_w = {}^3\mathbf{R}_4{}^T\ \mathbf{A}_s{}^T\ {}^0\mathbf{R}_7$$
$$\mathbf{B}_w = {}^3\mathbf{R}_4{}^T\ \mathbf{B}_s{}^T\ {}^0\mathbf{R}_7$$
$$\mathbf{C}_w = {}^3\mathbf{R}_4{}^T\ \mathbf{C}_s{}^T\ {}^0\mathbf{R}_7.$$

and now we can analytically extrapolate the joint positions of the wrist joints from the elements of the ${}^4\mathbf{R}_7(\theta_{5,6,7})$ matrix,

$${}^4\mathbf{R}_7(\theta_{5,6,7}) = \begin{bmatrix} * & * & \cos\theta_5\sin\theta_6 \\ * & * & \sin\theta_5\sin\theta_6 \\ -\sin\theta_6\cos\theta_7 & \sin\theta_6\sin\theta_7 & \cos\theta_6 \end{bmatrix}. \tag{21}$$

Respecting the global configuration parameter, we compute the remaining joint angles,

$$\theta_5 = \operatorname{atan2}\left(GC_6[a_{w23}\sin\psi + b_{w23}\cos\psi + c_{w23}],\; GC_6\left[a_{w13}\sin\psi + b_{w13}\cos\psi + c_{w13}\right]\right) \tag{22}$$

$$\theta_6 = GC_6 \arccos\left(a_{w33}\sin\psi + b_{w33}\cos\psi + c_{w33}\right) \tag{23}$$

$$\theta_7 = \operatorname{atan2}\left(GC_6[a_{w32}\sin\psi + b_{w32}\cos\psi + c_{w32}],\; GC_6\left[-a_{w31}\sin\psi - b_{w31}\cos\psi - c_{w31}\right]\right). \tag{24}$$

In conclusion, the joint angles are uniquely determined based on a target pose (${}^0\mathbf{T}_7$), and two auxiliary parameters, the arm angle (ψ) and the joint configuration (GC).

5. Joint Limits and Singularities

Joint limits and singularity avoidance are two crucial conditions to guarantee a stable and feasible motion in task space. The described method maps joint limits and singularities as intervals of the elbow redundancy circle; these intervals specify whether ψ will drive the robot to a joint limit violation or singularity violation (see Figure 4).

Feasible intervals are labeled $\Psi_{i,j}$, where the index indicates interval j of the i^{th} joint. The final interval (Ψ_{all}) is the intersection of the feasible intervals of all joints,

$$\Psi_{all} = \bigcap_{i=1}^{7}\Psi_i \qquad \text{and} \qquad \Psi_i = \bigcup_{j=1}^{n_j}\Psi_{i,j}. \tag{25}$$

The novelty of the proposed method has to do with the specification of the joint configuration when mapping the joint limits and singularities to the redundancy space. To determine these intervals, we will use the relation between joint angles and the elbow self-motion expressed in section 4. These relations are described in joints of pivot-type through a tangent function (17), (19), (22) and (24), and in joints of hinge-type through a cosine function (18) and (23). It is important to stress that the elbow joint angle, θ_4, does not depend on the arm angle and is therefore omitted from the following analysis.

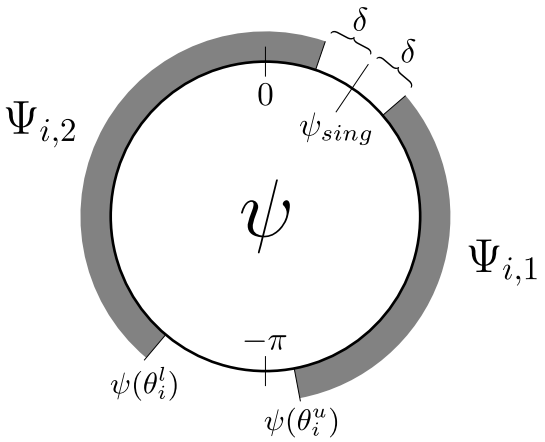

Figure 4: Example of joint limits and singularity intervals inscribed in the elbow redundancy circle for joint i. The $\psi(\theta_i^l)$ and $\psi(\theta_i^u)$ represent the arm angles where the respective joint limits are met, and ψ_{sing} is a singular arm configuration. An avoid interval is set next to the singular point with δ representing the unilateral spacing.

The expressions that represent the joint position, θ_i, as a function of the arm angle, ψ, can be summarized in two generic shapes: one for the pivot joints ($i = 1, 3, 5, 7$) where[2],

$$\begin{aligned}\theta_i(\psi) = \operatorname{atan2}(&GC_k\left[a_n \sin\psi + b_n \cos\psi + c_n\right], \\ &GC_k\left[a_d \sin\psi + b_d \cos\psi + c_d\right])\end{aligned} \tag{26}$$

and one for the hinge joints[3] ($i = 2, 6$),

$$\theta_i(\psi) = GC_k \arccos(a \sin\psi + b \cos\psi + c). \tag{27}$$

where $k = 2$ for $i \in \{1, 2, 3\}$ and $k = 6$ for $i \in \{5, 6, 7\}$. Having two generic functions to represent the relation between joint angles and the arm angle simplifies the analysis of the $\theta_i(\psi)$ function. It is possible to determine the intervals of ψ that correspond to feasible joint angles by solving these equations as a function of the joint limits, θ_i^l and θ_i^u. This is explained next.

5.1. Pivot Joints

In order to determine the arm angle intervals that map to the joint limits, or the singular arm angle, we need to differentiate these expressions. Simplifying the notation of (26) let $\theta_i(\psi) = \operatorname{atan2}(u, v)$, where

$$u = GC_k(a_n \sin\psi + b_n \cos\psi + c_n)$$

$$v = GC_k(a_d \sin\psi + b_d \cos\psi + c_d)$$

its total derivative[4] is given by,

$$\frac{d\theta_i}{d\psi} = \frac{\partial\theta_i}{\partial u}\frac{\partial u}{\partial\psi} + \frac{\partial\theta_i}{\partial v}\frac{\partial v}{\partial\psi} = \frac{vu'}{v^2+u^2} - \frac{uv'}{v^2+u^2}. \tag{28}$$

After simplification we obtain the following expression,

$$\frac{d\theta_i}{d\psi} = \frac{a_t \sin\psi + b_t \cos\psi + c_t}{v^2+u^2} \tag{29}$$

where,

$$a_t = GC_k(c_n b_d - b_n c_d)$$

[2] a_n, b_n and c_n are the signed coefficients of the first input of atan2 in equations (17), (19), (22) and (24), whereas index a_d, b_d and c_d represent the signed coefficients of the second input.

[3] a, b and c are the signed coefficients of acos in equations (18) and (23)

[4] In points where both partial derivatives exist, the function $\operatorname{atan2}(u, v)$ can be differentiated as $\arctan(u/v)$.

$$b_t = GC_k(a_n c_d - c_n a_d)$$
$$c_t = GC_k(a_n b_d - b_n a_d).$$

Using the Weierstrass-substitution method, the stationary points (ψ_0) are given, if they exist, by,

$$\psi_0 = 2\arctan\left(\frac{a_t \pm \sqrt{a_t^2 + b_t^2 - c_t^2}}{b_t - c_t}\right). \tag{30}$$

Depending on the value of $a_t^2 + b_t^2 - c_t^2$ three cases may arise:

- $a_t^2 + b_t^2 - c_t^2 > 0$, with stationary points;
- $a_t^2 + b_t^2 - c_t^2 < 0$, without stationary points;
- $a_t^2 + b_t^2 - c_t^2 = 0$, indeterminate joint angle.

5.1.1. With stationary points

The generic profiles of the function (26), when it has stationary points, is depicted in Figure 5. Stationary points represent the maximums, minimums or inflection points of the $\theta_i(\psi)$ function. Shimizu et al. [25] state that stationary points can be proved to be either global maximums or minimums, and elaborate on how the joint limits can be represented on the elbow redundancy circle, based on this premise (Figure 5a). This assumption, however,

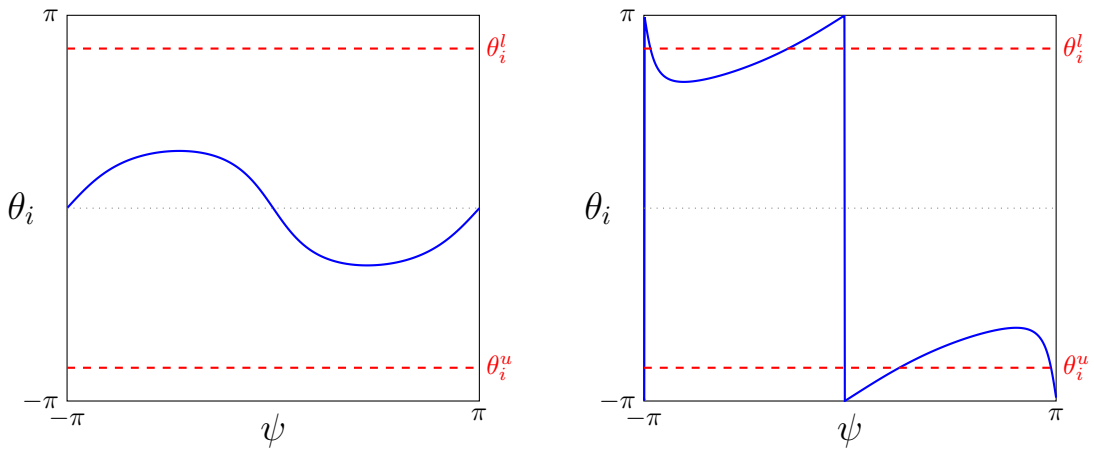

(a) Joint angle varies within $[-\pi, \pi]$.

(b) Joint angle variation crosses the $\{-\pi, \pi\}$ boundary.

Figure 5: Pivot joint $\theta_i(\psi)$ profile with stationary points.

cannot be extended to a general purpose manipulator. It is common in industrial manipulators to feature actuators with ample working range, close or even beyond the interval of $[-\pi, \pi]$. When the target pose and joint configuration (GC) are specified, the resulting joint positions may be near to a joint limit. Thus, a change in the arm angle may lead to a joint angle variation such that, $\theta_i(\psi) < -\pi \vee \theta_i(\psi) > \pi$. This leads to a discontinuity because the atan2 function maps the arm angle to the joint angle in the $[-\pi, \pi]$ range. When the joint angle overshoots this limit, the returned joint angle goes from π to $-\pi$ or vice-versa (see Figure 5b). Hence, the stationary points can not be considered global maximums or minimums.

5.1.2. Without stationary points

If the function is monotonic, there are no stationary points and there is a one-to-one correspondence between ψ and θ_i. The function $\theta_i(\psi)$ is not fully defined in the interval $[-\pi, \pi]$, due to the existence of a point of inversion, where the joint angle is discontinued (see Figure 6). This phenomenon has nothing to do with kinematic singularities, it derives from the range where atan2 maps the arm to the joint angle. Since the joint limits are commonly found within the $[-\pi, \pi]$ interval, this inversion occurs from outside the joint limits and causes no trouble.

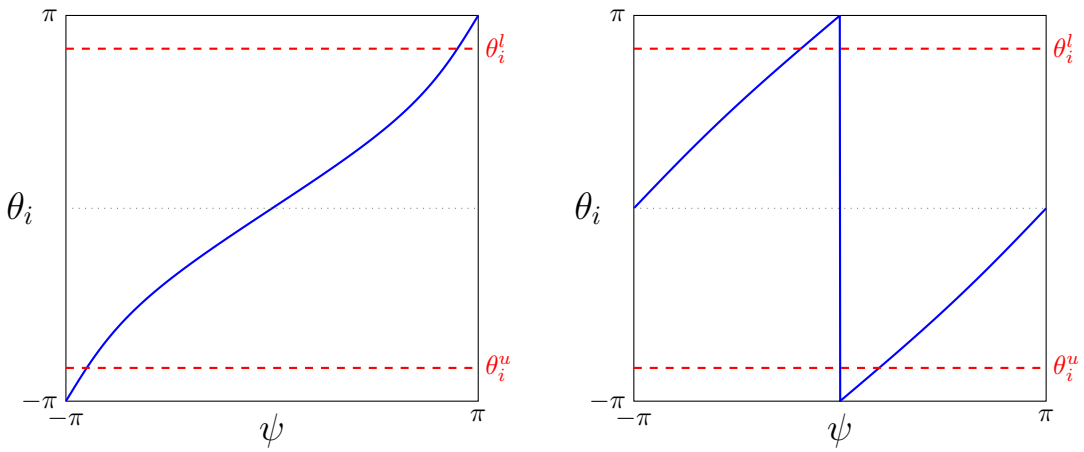

(a) Discontinuity of joint angle at $\psi = \{-\pi, \pi\}$.

(b) Discontinuity of joint angle at $\psi \in]-\pi, \pi[$.

Figure 6: Pivot joint $\theta_i(\psi)$ profile without stationary points.

5.1.3. Indeterminate Joint Angle

A singular point exists if the third condition is verified ($a_t^2 + b_t^2 - c_t^2 = 0$). The exact singular arm angle ψ_{sing} is directly determined from the stationary points of equation (30),

$$\psi_{sing} = 2 \arctan\left(\frac{a_t}{b_t - c_t}\right). \tag{31}$$

However, it cannot be labeled a stationary point because neither $\theta_i(\psi)$ nor its derivative is defined at that point. In a numerical approximation scheme it is not feasible to setup a condition that triggers on a single value due to

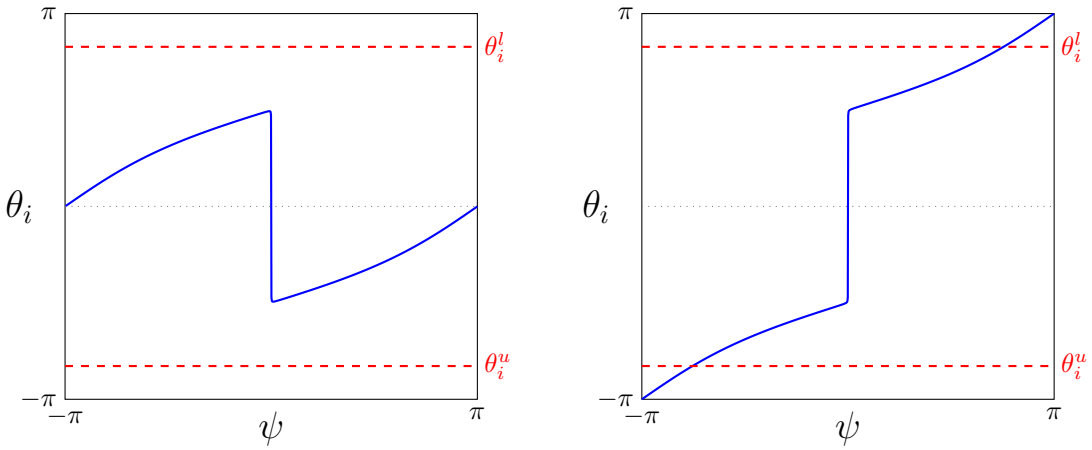

(a) Joint angle varies $-\pi$ at the singular arm angle.

(b) Joint angle varies π at the singular arm angle.

Figure 7: Pivot joint $\theta_i(\psi)$ profile when a singular arm angle exists.

inherent numerical errors. That being said, a tolerance threshold is usually defined to trigger whenever the value of $a_t^2 + b_t^2 - c_t^2$ approaches zero. A logic strategy to avoid singularities consists in avoiding intervals that contain the singular arm angle, $[\psi_{sing} - \delta, \psi_{sing} + \delta]$. The δ represents a constant value or a variable that depends on the defined tolerance threshold.

Now that we have identified and proposed a method to deal with singular arm angles, we still need a method to map the joint limits to the arm angle. A simple and effective way to achieve that, consists of solving (26) as a

function of the joint limits, θ_i^u and θ_i^l. Using the Weierstrass-substitution method we obtain,

$$\psi = 2\arctan\left(\frac{-b_p \pm \sqrt{b_p^2 - 4a_p c_p}}{2a_p}\right) \tag{32}$$

where,

$$\begin{aligned} a_p &= GC_k\left[(c_d - b_d)\tan(\theta_i) + (b_n - c_n)\right] \\ b_p &= 2\ GC_k[a_d\tan(\theta_i) - a_n] \\ c_p &= GC_k\left[(b_d + c_d)\tan(\theta_i) - (b_n + c_n)\right]. \end{aligned}$$

One of three outputs may occur:

- $\exists\psi \in [-\pi, \pi] :\ \theta_i(\psi) = \theta_i^l \vee \theta_i(\psi) = \theta_i^u$
- $\forall\psi \in [-\pi, \pi],\ \theta_i(\psi) \in \left]\theta_i^l, \theta_i^u\right[$
- $\forall\psi \in [-\pi, \pi],\ \theta_i(\psi) \notin \left[\theta_i^l, \theta_i^u\right]$.

If the first case is met, the $\psi(\theta_i^l)$ or $\psi(\theta_i^u)$ values are found, but that information alone does not specify if the function is entering an out-of-limits zone or an allowed zone. To do so, the first derivative of the function (29) is analyzed at these limit arm angles. If $\theta_i(\psi)$ and its derivative have the same sign at $\psi(\theta_i^l)$ or $\psi(\theta_i^u)$, the next interval will be an out-of-limits zone; else, if the sign differs the next joint angles will be within an allowed zone.

The last two cases occur if θ_i does not coincide with the joint limits, for any arm angle in the $[-\pi, \pi]$ interval. Assuming that $\theta_i(\psi)$ is defined in $[-\pi, \pi]$, any point along the function (26) will confirm if the whole interval is possible or not.

5.2. Hinge Joints

The same methodology used for pivot joints, is applied for hinge joints. The relation between joint and arm angle is represented by (27). Applying the derivative to $\theta_i(\psi)$ we obtain,

$$\frac{d\theta_i}{d\psi} = -GC_k\left(\frac{a\cos\psi - b\sin\psi}{\sin\theta_i}\right). \tag{33}$$

Using the Weierstrass-substitution again we calculate the stationary points,

$$\psi_0 = 2\arctan\left(\frac{-b \pm \sqrt{a^2 + b^2}}{a}\right). \tag{34}$$

The function exists in either $[-\pi, 0]$ or $[0, \pi]$ depending on the value of the configuration parameter, GC, for that particular joint. Depending on the value of $a^2 + b^2$ two cases may arise:

- $a^2 + b^2 > 0$, two stationary points;
- $a^2 + b^2 = 0$, one stationary point.

If the first condition is fulfilled, the hinge joint has a profile identical to the one depicted in Figure 8. Two stationary points exist in this case, one being the global minimum and the other the global maximum. Depending on the required pose and configuration parameter, the joint angle variation may be close to the joint limit, hence the need to check it for the hinge joints as well.

The arm is in a singular configuration when $\theta_2 = 0$ or $\theta_6 = 0$ hold. In such cases, $\theta_i(\psi)$ is still defined at that particular ψ value but the first derivative is not. For that reason, there is only one stationary point defined at a singular point (Figure 9), given by (34). If the configuration parameter (GC_k) is positive, the stationary point is the global maximum, else it is the global minimum.

Since $\theta_i(\psi)$ is continuous at a singular position (Figure 9), the singular arm angle in hinge joints does not need to be accounted for. Likewise to the pivot joints, equation (27) is solved as a function of the hinge joint limits to explore the associated arm angles.

$$\psi(\theta_i) = 2\arctan\left(\frac{a \pm \sqrt{a^2 + b^2 - (c - \cos\theta_i)^2}}{\cos\theta_i + b - c}\right) \tag{35}$$

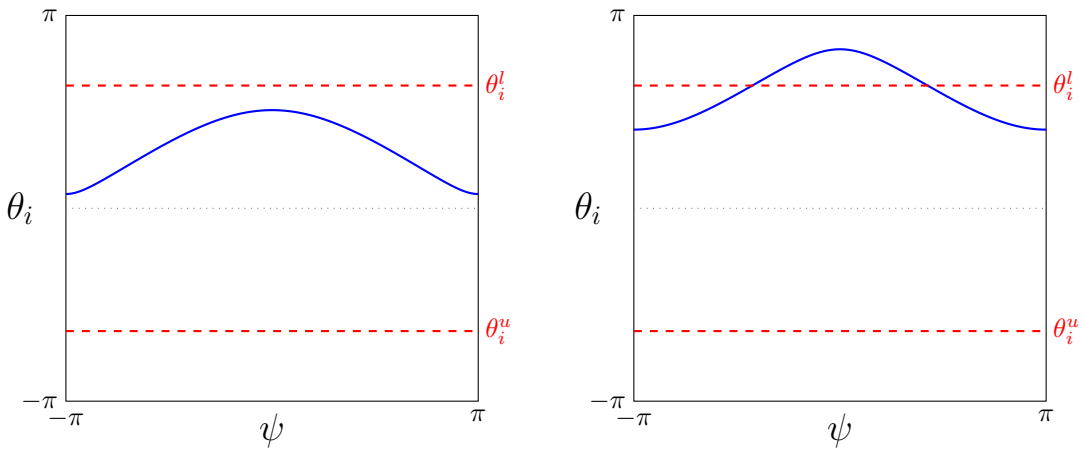

(a) Joint angle contained within joint limits.

(b) Joint angle crosses joint limits.

Figure 8: Hinge joint $\theta_i(\psi)$ profile when the configuration parameter is positive, function defined in $[0, \pi]$. If only the configuration is changed to a negative value, the function profile is mirrored relative to the x-axis.

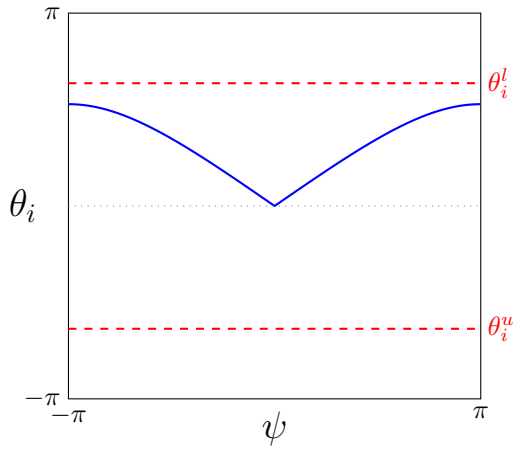

Figure 9: Hinge joint $\theta_i(\psi)$ profile when the arm is at a singular configuration.

The same outputs possible for the pivot joints are true for the hinge joints. If limits are crossed, we can check if the robot is entering an out-of-limits or an allowed zone by following the same metric – of the $\theta_i(\psi)$ and its derivative signs at the arm angles relative to the joint limit. If no limits are crossed, then any θ_i value can be used $\forall\psi \in [-\pi, \pi]$ to determine if the function is contained within the joint limits or if it is outside.

6. Redundancy Resolution

The proposed inverse kinematics algorithm receives as parameters: the desired end-effector pose (${}^0\mathbf{T}_7^d$), the global configuration of the manipulator (GC^d) and the arm angle (ψ). In this section, it will be proposed a redundancy resolution method to calculate the arm angle while avoiding joint limits and singularities.

The configuration control introduced in this paper is convenient in scenarios where the control loop is continuously performing inverse kinematics calculations for the robot to follow a given pose. In many applications like for instance human-robot interactions it is highly desirable that the robot follows a smooth and stable trajectory without sudden jumps between different configurations or passes through singular configurations in joint space.

The problem has been formulated such that the joint limits and singularities are projected into the redundancy circle by means of feasible arm angle intervals. As denoted in equations (25), each joint has associated to it a union of n_j feasible intervals, $\Psi_{i,j}$ (Figure 4), and the global feasible intervals (Ψ_{all}) develops from the intersection of each joint intervals, Ψ_i. The calculation of the arm angle is thus simplified since the only hard-constraints to the problem are the defined intervals.

A plausible approach to calculate the new arm angle (block "Calculate New ψ" in Figure 10) consists of applying a simple metric to the current arm angle, $\psi_{(t-1)}$, according to the current global feasible intervals. The current arm angle, can either be computed from the current joint positions θ_i^c (following the method explained in 3.2), or directly used from the preceding iteration.

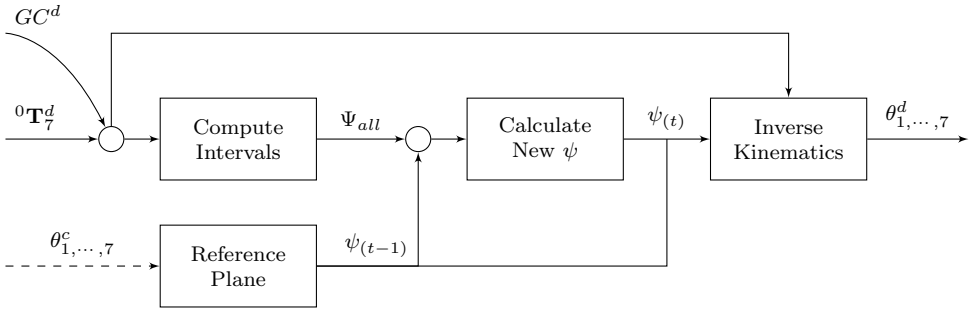

Figure 10: General control scheme for inverse kinematics resolution with joint limits and singularity avoidance.

First, we find the feasible interval that contains the previous arm angle $\left(\psi_{(t-1)} \in \Psi_{all,m},\ \Psi_{all,m} = [\psi_m^l, \psi_m^u]\right)$, (Figure 11). If the previous arm angle is contained in $\Psi_{all,m}$ the new arm angle can be computed as follows:

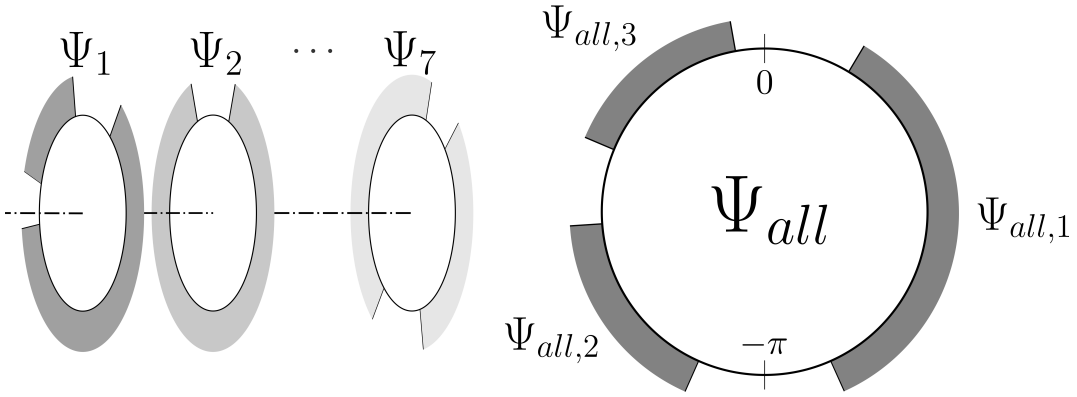

Figure 11: Example of intersection of feasible intervals from all the joints. The three resulting intervals are enumerated $m \in \{1, 2, 3\}$.

$$\psi_{(t)} = \psi_{(t-1)} + \mathrm{K}\left(\frac{\psi_m^u - \psi_m^l}{2}\right)\left[\mathrm{e}^{-\alpha\left(\frac{\psi_{(t-1)} - \psi_m^l}{\psi_m^u - \psi_m^l}\right)} - \mathrm{e}^{-\alpha\left(\frac{\psi_m^u - \psi_{(t-1)}}{\psi_m^u - \psi_m^l}\right)}\right] \tag{36}$$

where:

- $\mathrm{K} \in [0, 1]$, is a constant that controls the strength of repulsion of the arm angle from the limits;
- $\alpha \in \mathbb{R}^+$, is a constant that controls the distance to the limits from where the arm angle starts to repulse.

In case the previous arm angle is not contained in any feasible interval, either the elbow is moved to the closest feasible range, or the motion cannot be continued. This phenomenon is prone to happen when the trajectory has sparse poses or if the α value is too large, which permits the robot to move closer to its joint limits.

By changing α (cf. Figure 12), we can control the tendency of the arm angle to move towards the interval center or to preserve its position as long as it is distant from the limits. The problem of computing the new arm angle can also be tackled from an optimization standpoint, depending on the task requirements.

Finally, the parametrization of the manipulator redundancy as an ellipsoid that describes the elbow motion, has a clear representation in task space. Hence, it is straightforward to impose additional interval limits on the redundancy circle that relate to task space obstacles.

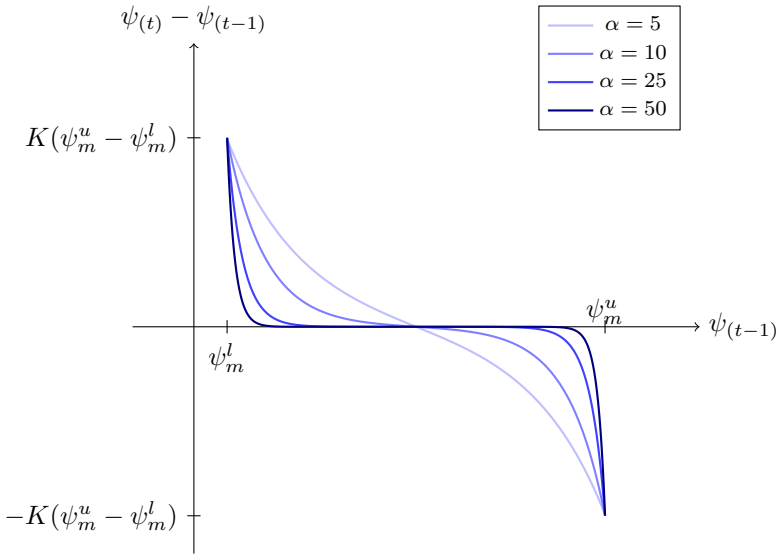

Figure 12: Change of the arm angle as a function of $\psi_{(t-1)}$, defined in the feasible interval $\Psi_{all,m}$.

6.1. Algorithm performance

The algorithm was implemented in MATLAB and C++ (Boost, Eigen) and the computational times were measured for the different parts of the above presented algorithm: i) the 'Inverse Kinematics' algorithm alone; ii) the 'Compute Intervals', joint limits and singularities mapping to the redundancy circle; and the complete algorithm, Figure10. Each algorithm was tested for a set of 10000 random and feasible poses. The performance of the algorithm was tested in a computer running Ubuntu 14.04 (Intel i7-4710MQ at 2.5GHz, 16GB of RAM).

Table 2: Descriptive statistics of computational times recorded of different parts of the algorithm, measured from 10000 samples, in microseconds (μs).

		Mean	Std. Deviation	Maximum
MATLAB	Inverse Kinematics	230.3	21.93	642.0
	Compute Intervals	822.3	88.61	622.0
	Full Algorithm	1132	77.65	3345
C++	Inverse Kinematics	2.247	1.228	32.00
	Compute Intervals	10.51	2.015	37.00
	Full Algorithm	12.74	2.103	43.00

6.2. Trajectory example

To demonstrate the redundancy resolution strategy, we created an example linear trajectory to be performed by the robot manipulator. The robot is purposely positioned at a configuration near its mechanical joint limits. The robot starts at the joint angles in degrees:

$$\theta^c = \begin{bmatrix} -5.4101 & -26.4986 & -48.1542 & -61.6500 & 152.6198 & 114.4466 & 8.1812 \end{bmatrix} \tag{37}$$

which correspond to the global configuration $GC = 3$, arm angle $\psi = 58.5882°$ and pose:

$${}^0\mathbf{T}_7^c = \begin{bmatrix} -0.2634 & -0.9112 & -0.3166 & -0.1174 \\ 0.3014 & -0.3895 & 0.8703 & -0.1464 \\ -0.9164 & 0.1338 & 0.3773 & 1.0203 \\ 0 & 0 & 0 & 1 \end{bmatrix} \tag{38}$$

The manipulator performs a linear motion in Cartesian space, keeping the same end-effector orientation but translating its position along the z-axis (${}^0\mathbf{R}_{7,z}$) of a distance of $0.25m$, ending at the target pose:

$${}^0\mathbf{T}_7^d = \begin{bmatrix} -0.2634 & -0.9112 & -0.3166 & -0.1966 \\ 0.3014 & -0.3895 & 0.8703 & 0.0712 \\ -0.9164 & 0.1338 & 0.3773 & 1.1146 \\ 0 & 0 & 0 & 1 \end{bmatrix} \tag{39}$$

The path is interpolated and a new pose is passed to the redundancy resolution algorithm (Figure10) every iteration. The global configuration remains unchanged throughout the trajectory, and the arm angle varies according to the parameters defined (α and K)[5].

First, the impact of the parameter α is evaluated. Keeping the parameter $K = 0.1$ constant in all tests, we depict how different values of α affect the arm angle motion along the trajectory (Figure13a). Then, the value of α is fixated at 20 and the effect of different values of K is demonstrated (Figure13b). The evolution of the joint angles along the trajectory for each of the tests ran is depicted (Figure13c and 13d).

7. Conclusion and Future Work

In this paper we introduced the concept of global joint configuration control in position-based inverse kinematics calculation. The same parameter that defines the global joint configuration was applied when deriving the expressions of the joint angles as a function of the arm angle.

The relation of the joint angles with the arm angle and global configuration enabled the mapping of the joint limits and singularities in the nullspace represented by the redundancy circle. It was shown a method to reliably compute intervals of feasible elbow positions to avoid joint limits and singularities. A simple metric to compute the arm angle from the interval of feasible arm angles was also discussed.

Being an analytic solution, the time required for each operation is limited and quantifiable, which makes this method adequate for real-time control systems. This solution relies on simple mathematical operations that are implemented and fully optimized in mathematical software libraries, making it a very light and fast algorithm.

The proposed algorithm is specifically relevant in scenarios where the task execution requires continuous and predictable motion execution, avoiding jumping between configurations, passing singularities or reaching joint limits. One possible application is human-robot collaboration tasks where the motions performed by the robot are need to be validated before-hand, for example in robotic-surgery tasks. Some of the robotic tasks performed in surgical scenarios are defined in a pre-operation stage, and the controller should guarantee that the robot motion is safe, predictable and complete [31]. Another possible application regards haptic or hands-on manipulator control of the manipulator that relies on continuous position-based inversion of the task space coordinates to the joint space. A simple metric, such as the one introduced in section 6 can be applied to keep the robot away from joint limits and singularities while continuously following the new target pose.

As future work, the authors will evaluate the efficiency of the proposed method embedded in a robotic controller. The algorithm, as-is, generates the exact joint coordinates that map to a desired pose and configuration. This solution however, does not compensate for the manipulator's compliance errors, which are specially relevant when the manipulator's works under variant force payloads [32, 33].

Acknowledgments

This work was partially supported by the NETT Project [FP7-PEOPLE-2011-ITN-289146]; and Foundation for Science and Technology, Portugal [grant number SFRH/BD/86499/2012].

Appendix I. Conventional Denavit-Hartenberg matrices of a S-R-S 7-DoF manipulator

The conventional Denavit-Hartenberg matrices for a S-R-S 7-DoF manipulator (cf. section 3) are shown here:

$${}^0\mathbf{T}_1 = \begin{bmatrix} \cos\theta_1 & 0 & -\sin\theta_1 & 0 \\ \sin\theta_1 & 0 & \cos\theta_1 & 0 \\ 0 & -1 & 0 & d_{bs} \\ 0 & 0 & 0 & 1 \end{bmatrix} \tag{40}$$

[5]Motion comparison with different values of α and K in video format – (`https://youtu.be/mcMfWkMP1hQ`).

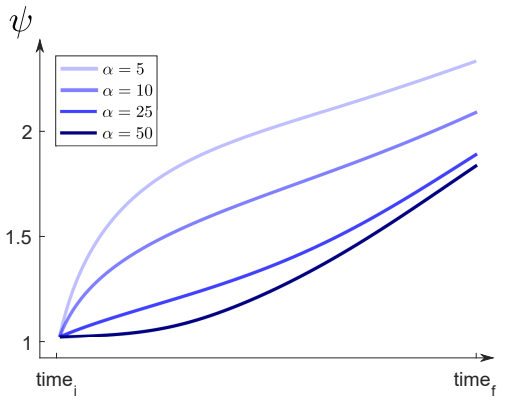

(a) Different values of α and $K = 0.1$.

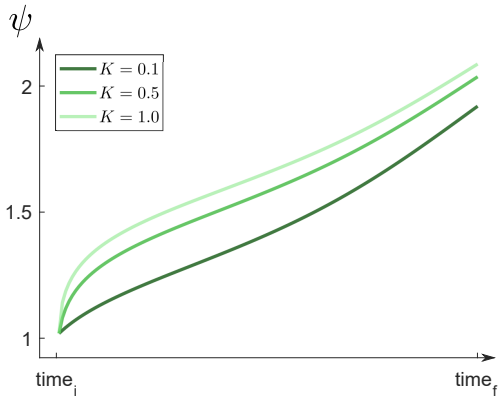

(b) Different values of K and $\alpha = 20$.

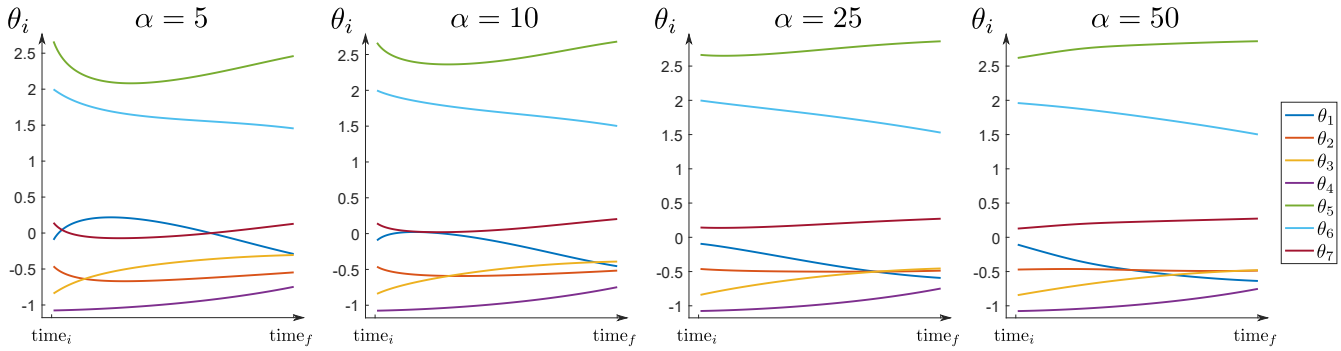

(c) Variation of the joint angles for different values of α ($K = 0.1$).

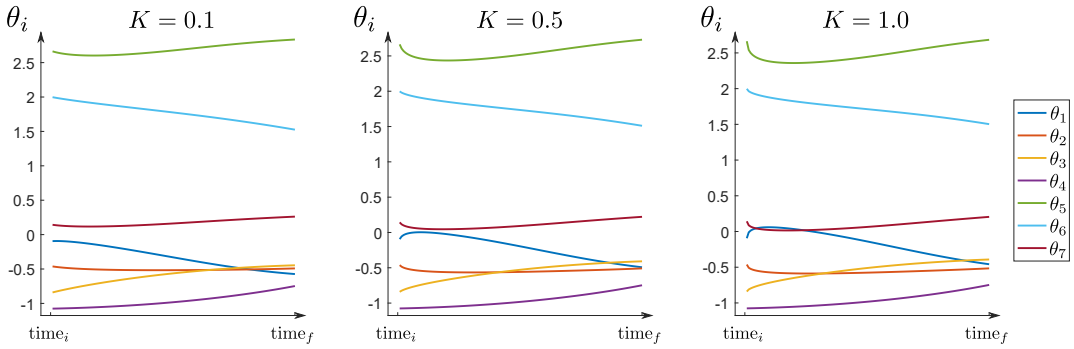

(d) Variation of the joint angles for different values of K ($\alpha = 20$).

Figure 13: Variation of the arm angle (ψ) and joint angles along the trajectory.

$$ {}^{1}\mathbf{T}_2 = \begin{bmatrix} \cos\theta_2 & 0 & \sin\theta_2 & 0 \\ \sin\theta_2 & 0 & -\cos\theta_2 & 0 \\ 0 & 1 & 0 & 0 \\ 0 & 0 & 0 & 1 \end{bmatrix} \tag{41} $$

$$ {}^{2}\mathbf{T}_3 = \begin{bmatrix} \cos\theta_3 & 0 & \sin\theta_3 & 0 \\ \sin\theta_3 & 0 & -\cos\theta_3 & 0 \\ 0 & 1 & 0 & d_{se} \\ 0 & 0 & 0 & 1 \end{bmatrix} \tag{42} $$

$$
{}^{3}\mathbf{T}_{4} = \begin{bmatrix} \cos\theta_4 & 0 & -\sin\theta_4 & 0 \\ \sin\theta_4 & 0 & \cos\theta_4 & 0 \\ 0 & -1 & 0 & 0 \\ 0 & 0 & 0 & 1 \end{bmatrix} \tag{43}
$$

$$
{}^{4}\mathbf{T}_{5} = \begin{bmatrix} \cos\theta_5 & 0 & -\sin\theta_5 & 0 \\ \sin\theta_5 & 0 & \cos\theta_5 & 0 \\ 0 & -1 & 0 & d_{ew} \\ 0 & 0 & 0 & 1 \end{bmatrix} \tag{44}
$$

$$
{}^{5}\mathbf{T}_{6} = \begin{bmatrix} \cos\theta_6 & 0 & \sin\theta_6 & 0 \\ \sin\theta_6 & 0 & -\cos\theta_6 & 0 \\ 0 & 1 & 0 & 0 \\ 0 & 0 & 0 & 1 \end{bmatrix} \tag{45}
$$

$$
{}^{6}\mathbf{T}_{7} = \begin{bmatrix} \cos\theta_7 & -\sin\theta_7 & 0 & 0 \\ \sin\theta_7 & \cos\theta_7 & 0 & 0 \\ 0 & 0 & 1 & d_{wf} \\ 0 & 0 & 0 & 1 \end{bmatrix} \tag{46}
$$

Appendix II. Nomenclature

Constants

α	Constant that controls the distance to the limits from where the arm angle starts to repulse from the feasible interval limits, $\alpha \in R^{+}$
δ	User-defined scalar that represents half of the avoid interval range around a singular arm angle (ψ_{sing})
θ_i^l	Lower position limit of the joint i
θ_i^u	Upper position limit of the joint i
d_{bs}	Euclidean distance from the base coordinate frame ($\mathbf{T}_0$) to the shoulder coordinate frame ($\mathbf{T}_2$)
d_{ew}	Euclidean distance from the elbow coordinate frame ($\mathbf{T}_4$) to the wrist coordinate frame ($\mathbf{T}_6$)
d_{se}	Euclidean distance from the shoulder coordinate frame ($\mathbf{T}_2$) to the elbow coordinate frame ($\mathbf{T}_4$)
d_{wf}	Euclidean distance from the wrist coordinate frame ($\mathbf{T}_6$) to the flange coordinate frame ($\mathbf{T}_7$)
K	Constant that controls the strength of repulsion of the arm angle from the feasible interval limits, $K \in [0, 1]$

Notation

$[\hat{\mathbf{v}}\times]$	Cross-product matrix for the unit vector $\hat{\mathbf{v}}$
$\mathbf{I}_n$	Identity matrix of size $n \times n$
$\mathbf{v}_{abc}$	Vector normal to the plane ABC
${}^{i}\mathbf{p}_j$	Position of the coordinate frame $\mathbf{T}_j$ with respect to the coordinate frame $\mathbf{T}_i$
${}^{i}\mathbf{p}_{j,x}$	Coordinate x of the vector ${}^{i}\mathbf{p}_j$
${}^{i}\mathbf{R}_j$	Rotation of the coordinate frame $\mathbf{T}_j$ with respect to the coordinate frame $\mathbf{T}_i$
${}^{i}\mathbf{R}_{j,z}$	Z-axis of the rotation frame ${}^{i}\mathbf{R}_j$ (3^{rd} column)
${}^{i}\mathbf{T}_j$	Transformation of the coordinate frame $\mathbf{T}_j$ with respect to the coordinate frame $\mathbf{T}_i$
ABC	Plane formed by three non-collinear points A, B and C
m_{ij}	Element of the matrix $\mathbf{M}$ at the i^{th} line and j^{th} column

$\text{sgn}(x)$ Sign of scalar value x

Variables

ϕ Angle formed by the shoulder-wrist vector ($^2\mathbf{p}_6$) and the shoulder-elbow vector ($^2\mathbf{p}_4$)

ψ Arm angle parameter, represents the angle formed by the shoulder-elbow-wrist plane (SEW) and the reference plane

ψ_m^l Lower limit of the feasible interval ψ_m

ψ_m^u Upper limit of the feasible interval ψ_m

ψ_0 Stationary points of the function $\frac{d\theta_i}{d\psi}$, (29)

$\Psi_a ll$ Intersection of the 'union of feasible intervals (Ψ_i)' from all the joints

$\Psi_a ll, m$ The m^{th} interval of $\Psi_a ll$. Also referred to as ψ_m

Ψ_i Union of all feasible intervals of the i^{th} joint

$\psi_{(t)}$ Next iteration arm angle

$\psi_{(t-1)}$ Current iteration arm angle

$\Psi_{i,j}$ Interval of feasible arm angles, indicating the j^{th} interval of the i^{th} joint

ψ_{sing} Arm angle at a singular configuration

θ_i^c Current position of the joint i

θ_i^d Desired position of the joint i

θ_i^v Position of the joint i of the virtual manipulator

θ_i Position of the joint i

a, b, c Signed coefficients of of acos in equations (18) and (23)

a_d, b_d, c_d Signed coefficients of the second input of atan2 in equations (17), (19), (22) and (24)

a_n, b_n, c_n Signed coefficients of the first input of atan2 in equations (17), (19), (22) and (24)

References

[1] J. M. Hollerbach, Optimum kinematic design for a seven degree of freedom manipulator, Tech. rep., MIT Artificial Intellegence Laboratory, Cambridge (1985).

[2] D. DeMers, K. Kreutz-Delgado, Global Regularization of Inverse Kinematics for Redundant Manipulators, Advances in Neural Information Processing Systems 5 (1993) 255—-262.

[3] D. DeMers, K. Kreutz-Delgado, Learning Global Topological Properties of Robot Kinematic Mappings for Neural Network-based Configuration Control, in: Neural Networks in Robotics, Springer US, Boston, MA, 1993, pp. 3–17. doi:10.1007/978-1-4615-3180-7_1.

[4] J. W. Burdick, On the inverse kinematics of redundant manipulators: characterization of the self-motion manifolds, in: International Conference on Robotics and Automation, IEEE Comput. Soc. Press, Scottsdale, 1989, pp. 264–270. doi:10.1109/ROBOT.1989.99999.

[5] C. L. Luck, S. Lee, Self-motion topology for redundant manipulators with joint limits, in: International Conference on Robotics and Automation, IEEE Comput. Soc. Press, Atlanta, 1993, pp. 626–631. doi:10.1109/ROBOT.1993.291835.

[6] K. Kreutz-Delgado, M. Long, H. Seraji, Kinematic Analysis of 7-DOF Manipulators, The International Journal of Robotics Research 11 (5) (1992) 469–481. doi:10.1177/027836499201100504.

[7] B. Tondu, A closed-form inverse kinematic modelling of a 7R anthropomorphic upper limb based on a joint parametrization, in: International Conference on Humanoid Robots, IEEE, Genoa, 2006, pp. 390–397. doi:10.1109/ICHR.2006.321302.

[8] H. H. An, W. I. Clement, B. Reed, Analytical inverse kinematic solution with self-motion constraint for the 7-DOF restore robot arm, in: International Conference on Advanced Intelligent Mechatronics, IEEE, Besançon, 2014, pp. 1325–1330. doi:10.1109/AIM.2014.6878266.

[9] H. Seraji, Configuration control of redundant manipulators: theory and implementation, IEEE Transactions on Robotics and Automation 5 (4) (1989) 472–490. doi:10.1109/70.88062.

[10] S. Chiaverini, Singularity-robust task-priority redundancy resolution for real-time kinematic control of robot manipulators, IEEE Transactions on Robotics and Automation 13 (3) (1997) 398–410. doi:10.1109/70.585902.

[11] L. Yan, Z. Mu, W. Xu, Analytical inverse kinematics of a class of redundant manipulator based on dual arm-angle parameterization, in: International Conference on Systems, Man, and Cybernetics (SMC), IEEE, San Diego, 2014, pp. 3744–3749. doi:10.1109/SMC.2014.6974513.

[12] D. N. Nenchev, Y. Tsumaki, M. Takahashi, Singularity-consistent kinematic redundancy resolution for the S-R-S manipulator, in: 2004 IEEE/RSJ International Conference on Intelligent Robots and Systems (IROS) (IEEE Cat. No.04CH37566), Vol. 4, IEEE, 2004, pp. 3607–3612. doi:10.1109/IROS.2004.1389975.

[13] T. F. Chan, R. V. Dubey, A weighted least-norm solution based scheme for avoiding joint limits for redundant joint manipulators, IEEE Transactions on Robotics and Automation 11 (2) (1995) 286–292. doi:10.1109/70.370511.

[14] Z.-L. Zhou, C. C. Nguyen, Joint configuration conservation and joint limit avoidance of redundant manipulators, in: International Conference on Robotics and Automation, Vol. 3, IEEE, Albuquerque, 1997, pp. 2421–2426. doi:10.1109/ROBOT.1997.619324.

[15] B. J. Nelson, P. K. Khosla, Strategies for Increasing the Tracking Region of an Eye-in-Hand System by Singularity and Joint Limit Avoidance, The International Journal of Robotics Research 14 (3) (1995) 255–269. doi:10.1177/027836499501400304.

[16] R. Colbaugh, H. Seraji, K. L. Glass, Obstacle avoidance for redundant robots using configuration control, Journal of Robotic Systems 6 (6) (1989) 721–744. doi:10.1002/rob.4620060605.

[17] Y. Nakamura, H. Hanafusa, T. Yoshikawa, Task-Priority Based Redundancy Control of Robot Manipulators, The International Journal of Robotics Research 6 (2) (1987) 3–15. doi:10.1177/027836498700600201.

[18] K. Suh, J. Hollerbach, Local versus global torque optimization of redundant manipulators, in: International Conference on Robotics and Automation, Vol. 4, IEEE, Raleigh, 1987, pp. 619–624. doi:10.1109/ROBOT.1987.1087955.

[19] T. Yoshikawa, Manipulability and redundancy control of robotic mechanisms, in: International Conference on Robotics and Automation, Vol. 2, Institute of Electrical and Electronics Engineers, St. Louis, 1985, pp. 1004–1009. doi:10.1109/ROBOT.1985.1087283.

[20] T. Asfour, R. Dillmann, Human-like motion of a humanoid robot arm based on a closed-form solution of the inverse kinematics problem, in: International Conference on Intelligent Robots and Systems, Vol. 2, IEEE, Las Vegas, 2003, pp. 1407–1412. doi:10.1109/IROS.2003.1248841.

[21] H. Kim, J. Rosen, Predicting Redundancy of a 7 DOF Upper Limb Exoskeleton Toward Improved Transparency between Human and Robot, Journal of Intelligent & Robotic Systems 80 (S1) (2015) 99–119. doi:10.1007/s10846-015-0212-4.

[22] Y. Nakamura, H. Hanafusa, Inverse Kinematic Solutions With Singularity Robustness for Robot Manipulator Control, Journal of Dynamic Systems, Measurement, and Control 108 (3) (1986) 163. doi:10.1115/1.3143764.

[23] P. Chang, A closed-form solution for inverse kinematics of robot manipulators with redundancy, IEEE Journal on Robotics and Automation 3 (5) (1987) 393–403. doi:10.1109/JRA.1987.1087114.

[24] D. Tolani, A. Goswami, N. I. Badler, Real-Time Inverse Kinematics Techniques for Anthropomorphic Limbs, Graphical Models 62 (5) (2000) 353–388. doi:10.1006/gmod.2000.0528.

[25] M. Shimizu, H. Kakuya, W.-K. Yoon, K. Kitagaki, K. Kosuge, Analytical Inverse Kinematic Computation for 7-DOF Redundant Manipulators With Joint Limits and Its Application to Redundancy Resolution, IEEE Transactions on Robotics 24 (5) (2008) 1131–1142. doi:10.1109/TRO.2008.2003266.

[26] S. Lee, A. Bejczy, Redundant arm kinematic control based on parameterization, in: International Conference on Robotics and Automation, IEEE Comput. Soc. Press, Sacramento, 1991, pp. 458–465. doi:10.1109/ROBOT.1991.131621.

[27] P. Dahm, F. Joublin, Closed form solution for the inverse kinematics of a redundant robot arm (1997).

[28] I. Kuhlemann, A. Schweikard, P. Jauer, F. Ernst, Robust inverse kinematics by configuration control for redundant manipulators with seven DoF, in: International Conference on Control, Automation and Robotics, IEEE, Hong Kong, 2016, pp. 49–55. doi:10.1109/ICCAR.2016.7486697.

[29] H. Moradi, S. Lee, Joint Limit Analysis and Elbow Movement Minimization for Redundant Manipulators Using Closed Form Method, in: International Conference on Intelligent Computing, Springer, Berlin, Heidelberg, 2005, pp. 423–432. doi:10.1007/11538356_44.

[30] G. K. Singh, J. Claassens, An analytical solution for the inverse kinematics of a redundant 7DoF Manipulator with link offsets, in: International Conference on Intelligent Robots and Systems, IEEE, Taipei, 2010, pp. 2976–2982. doi:10.1109/IROS.2010.5649095.

[31] C. Faria, W. Erlhagen, M. Rito, E. De Momi, G. Ferrigno, E. Bicho, Review of Robotic Technology for Stereotactic Neurosurgery, IEEE Reviews in Biomedical Engineering 8 (2015) 125–137. doi:10.1109/RBME.2015.2428305.

[32] A. Klimchik, A. Pashkevich, Serial vs. quasi-serial manipulators: Comparison analysis of elasto-static behaviors, Mechanism and Machine Theory 107 (February 2016) (2017) 46–70. doi:10.1016/j.mechmachtheory.2016.09.019.

[33] A. Klimchik, A. Ambiehl, S. Garnier, B. Furet, A. Pashkevich, Efficiency evaluation of robots in machining applications using industrial performance measure, Robotics and Computer-Integrated Manufacturing 48 (October 2015) (2017) 12–29. doi:10.1016/j.rcim.2016.12.005.